Effect of Wing/Canard Interference on the Loading of a Delta Wing

J. Er-El*
Technion—Israel Institute of Technology, Haifa, Israel

The effect of canard interference on the loading of a delta wing is studied in this work. It is shown that, as a result of the wing/canard interference, the suction induced by the wing vortices decreases in the apex region and increases downstream of it. When the canard sweep angle is sufficiently large, the canard vortices induce suction directly on the wing upper surface. In this case, the breakdown of the canard vortices is followed by stall-like characteristics of the wing. A decrease in the longitudinal separation of the wing and the canard results in an increase in the region of reduced suction in the vicinity of the apex. This can weaken the downstream development of the wing vortices and the suction induced by them, consequently decreasing the normal force of the main wing.

Nomenclature

A	=	wing area
c	=	wing root chord
C_M	=	pitching moment coefficient, relative to the wing apex
C_N	=	normal force coefficient
C_p	=	pressure coefficient $[(p-p_\infty)/q]$
p	=	pressure
q	=	dynamic pressure
$s(\bar{x})$	=	wing local semispan
$\bar{x}$	=	nondimensional chordwise coordinate ($\bar{x}=x/c$), see Fig. 4
$\bar{y}$	=	nondimensional local spanwise coordinate $[\bar{y}=y/s(\bar{x})]$, see Fig. 4
$\bar{z}$	=	nondimensional vertical coordinate ($\bar{z}=z/c$), see Fig. 4
α	=	angle of attack

Superscripts

ℓ	=	at the lower surface
u	=	at the upper surface

Subscripts

min	=	minimum
∞	=	freestream

Introduction

CLOSE-COUPLED delta wing/canard configurations for trisonic aircraft have been in operation for the past two decades. These configurations offer high trimmed lift, improved maneuverability, and a potential for increased lift-to-drag ratio, all of which make them attractive for present as well as for future aircraft.

The first study of the wing/canard interference mechanism, the results of which were incorporated in the aerodynamic design of the SAAB-Viggen, was carried out by Behrbohm.[1] Subsequent studies by Gloss and McKinney[2] and Campbell et al.[3] consisted of parametric studies on delta wing/canard/fuselage configurations and were based mostly on force and moment measurements. The integrated character of the results obtained in these studies did not explain the details of the wing/canard interference mechanism or its effect on the wing loading. Miner and Gloss[4] carried out a flow visualization study that showed that wing/canard interference delayed the onset of vortex breakdown on the wing vortices to higher incidence angles. Gloss and Washborn[5] measured surface pressures on a wing/canard/fuselage configuration at transonic speeds and at an angle-of-attack range in which the effect of vortex breakdown on the wing vortices is small or nonexistent (4–16 deg). Er-El and Seginer[6] studied the interaction of the delta wing and canard leading-edge vortices, in the incidence range of 12–30 deg. In this range, the vortex interaction and vortex breakdown play a prominent role in the interference mechanism. The latter study is based on measurement of the leading-edge vortex trajectories of the wing and canard, as well as force and moment measurements. Their results show that although the canard presence delayed the onset of vortex breakdown, in some cases the wing-canard configuration stalled at a lower angle of attack than the wing alone.

The purpose of the present research is to study the effects of delta wing/canard interference and its manifestation on the surface pressures as well as on the normal force and pitching moment of the wing. The study is carried out for configurations that are geometrically similar to those used in Ref. 6. This choice enables the use of the vortex trajectory data presented there in conjunction with the pressure data. Thus, one can examine the relation between the changes in the vortex trajectories caused by wing/canard interference, the corresponding changes in the pressures induced by these vortices, and the normal force and pitching moment of the wing.

Experimental Setup and Procedure

The experiments were carried out in the 1×1 m^2 subsonic wind tunnel of the Aeronautical Research Center at Technion, at an airspeed of 32 m/s and Reynolds number of approximately 0.5×10^6, based on wing root chord. These experiments consisted of detailed static pressure measurements on the surfaces of the wing in the wing/canard configurations tested.

The wing and the canards used in this study are shown in Fig. 1. The wing is a sharp-edged flat plate, with a delta planform of 60 deg sweep angle. It has a root chord length of 24.6 cm, uniform thickness of 4.6 mm, and symmetrical, wedge-

Received Nov. 11, 1985; revision received May 22, 1987.

*Senior Lecturer, Department of Aeronautical Engineering.

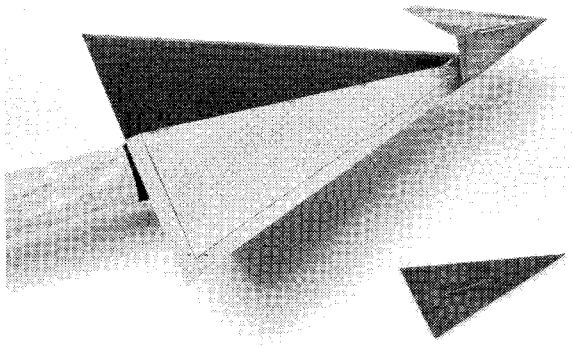

Fig. 1 Wing and canard models (the wing/MS canard configuration is assembled).

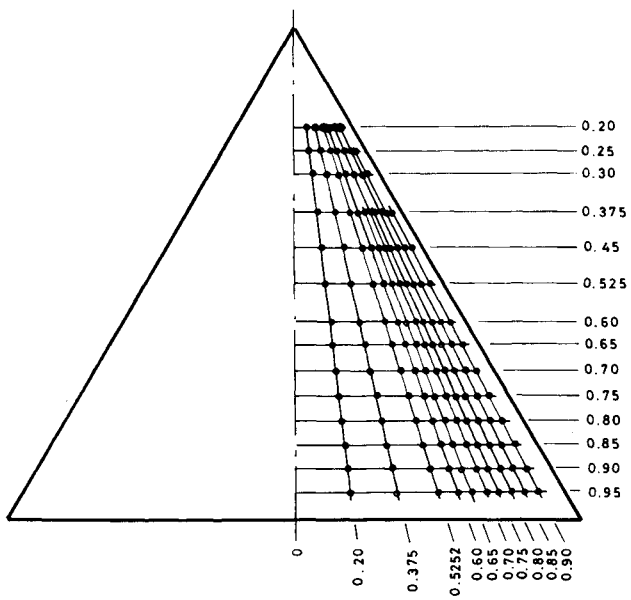

Fig. 2 Map of the pressure holes on the wing.

shaped (apex angle of 30 deg) leading and trailing edges. The leading- and trailing-edge profiles used here are different from those used in Ref. 6. There, the upper surface of the leading edge is flush with the wing surface and the lower surface is inclined toward the leading-edge apex to form an apex angle of 30 deg (see Fig. 4). Pressure tubes, of 0.6 mm inside diameter, are embedded in the wing, and 130 ports for pressure measurements are drilled on the upper surface, in an arrangement depicted in Fig. 2.

The two canards are flat, sharp-edged planforms, 1.5 mm thick. The moderately swept (MS) canard is a cropped-arrow planform with a leading-edge sweep angle of 50 deg, a trailing-edge sweep angle of 40 deg, a span of 96 mm, and a root chord length of 65 mm. The highly swept (HS) canard is a delta wing, with a leading-edge sweep angle of 75 deg, a straight trailing edge, and a span of 58.5 mm. The areas of the two canards are almost equal: 33 and 32 cm^2 for the MS and HS canards, respectively. The canards are joined to the wing by a flat strut of 1.5 mm thickness with sharp, wedge-shaped leading and trailing edges.

Table 1 Configurations tested and relative positions of wing and canard.

No. configuration	Canard position: Vertical $\bar{z}$	Canard position: Longitudinal $\bar{x}$
I Wing-alone	N/A	N/A
II Wing/MS canard	0.088	-0.130
III Wing/HS canard, forward position	0.088	-0.295
III Wing/HS canard, rear position	0.088	-0.265

[a] The position of the canard apex relative to the wing apex, nondimensionalized with respect to the wing root chord.

Table 1 presents a list of the configurations tested and the positions of the canards relative to the main wing apex. Configurations II and III in the present work are geometrically similar to the configuration with the MS canard in the forward position and the configuration with the HS canard, respectively, used in Ref. 6.

The pressure measurement system is based on three 48-port scanivalve modules, each connected to a pressure transducer. This system provides the readings of the surface pressures, the freestream dynamic pressure, and a calibration pressure of 10.16 cm (4 in.) water. The calibration pressure was determined by a micromanometer with resolution of ± 0.001 in. water. A detailed description of the experimental setup is given in Ref. 7.

The experiments were carried out in the incidence range of 0–32 deg. In each experiment, the reading of the calibration pressure was obtained by each of the pressure transducers. An experiment was considered acceptable when the difference between each of these readings and the micromanometer reading did not exceed 1%. The pressure measurements on the wing alone, which are used for both reference and comparison, were obtained from Ref. 7. These measurements were done on the same wing used in the present study. Initial tests on the wing/canard configurations showed that the effects of wing/canard interference are significant only on the upper (suction) surface of the main wing; the pressure distributions on the lower surface are similar to those of the wing alone reported in Ref. 7. Consequently, the pressures were measured only on the upper surface of the wing.

Results and Discussions

Effects of Canard Presence

Figure 3 features spanwise pressure profiles for the wing-alone and wing/HS canard (the canard in the forward position) configurations.

It is useful to precede the present results with a brief presentation of some results from a previous work[6] relevant to this study. Reference 6 is an experimental study on the effect of the canard presence on the trajectories and the breakdown of the leading-edge vortices of the wing and the canard. The main features of this effect are represented qualitatively in Fig. 4. It shows that canard presence alters the wing leading-edge vortex trajectories.

The changes in the leading-edge vortex trajectories due to the presence of the canard are evident in the pressure distributions. Comparison of the spanwise position of the suction peaks shows that in the wing/canard configuration these peaks are, in general, outboard to those in the wing-alone configuration. This is consistent with the larger spanwise component observed (Fig. 4) for the wing vortex trajectories in the wing/canard configuration.[6] Note that in the apex region, at $\alpha = 10$ deg, this larger spanwise component caused the suction peaks in the wing/canard configuration to be displaced outboard of the pressure ports array. Consequently, they do not appear in the spanwise C_p^u profile at $\bar{x} = 0.25$.

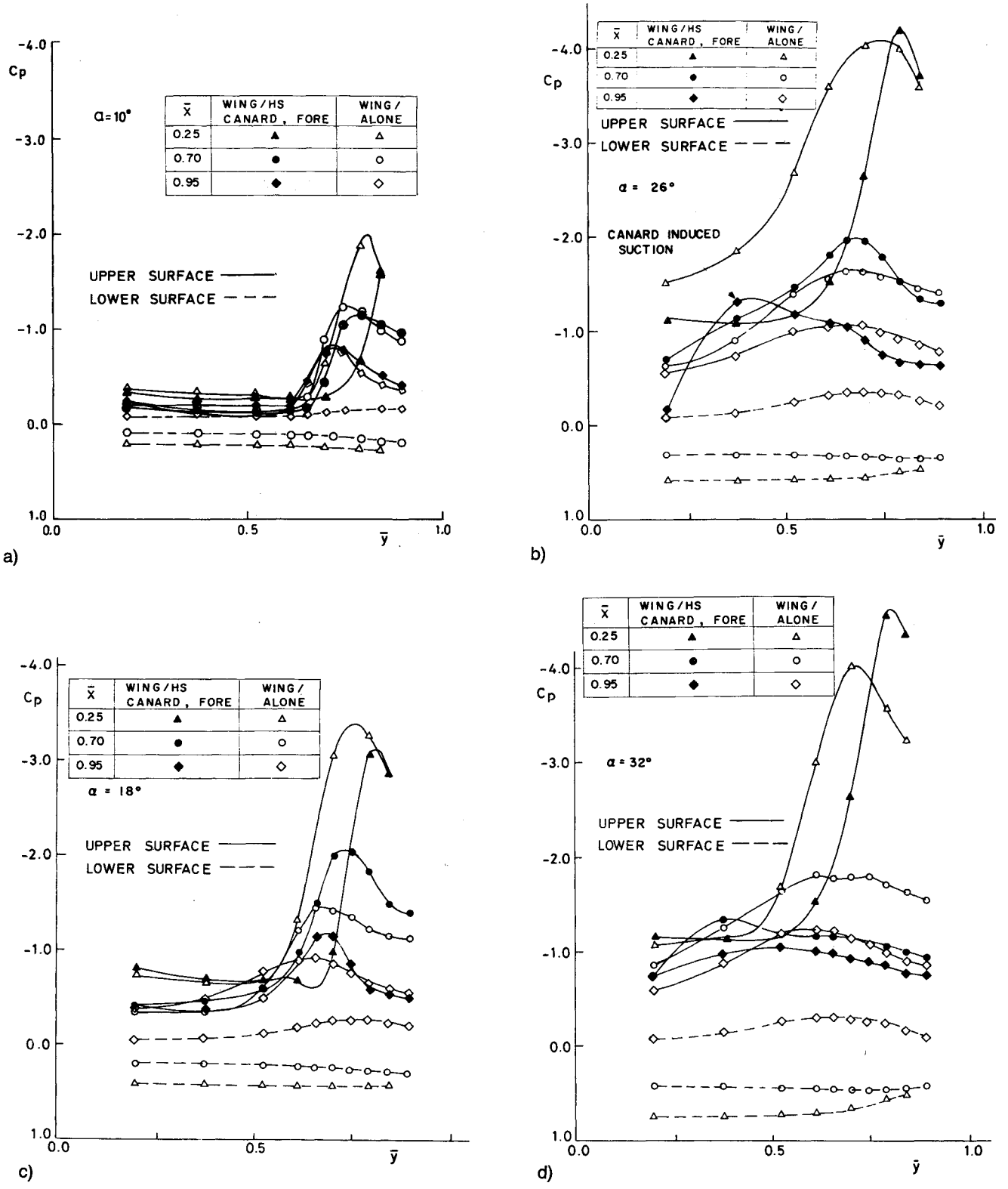

Fig. 3 Spanwise pressure distribution of the wing-alone and the wing/HS canard in the forward position configurations: a) $\alpha = 10$ deg. b) $\alpha = 18$ deg. c) $\alpha = 26$ deg. d) $\alpha = 32$ deg.

Comparison of the magnitude of $C^{u}_{p,\min}$ in the suction peaks in the two configurations shows that canard-presence effects vary with the chordwise position. In the vicinity of the apex (represented by $\bar{x} = 0.25$), the presence of the canard reduces the maximum suction as long as vortex bursting has not reached this region (e.g., $\alpha = 10$ and 18 deg, Figs. 3a and 3b). At these angles, the reduction is due to the downwash of the canard on the wing. This is consistent with the lower vertical position of the wing vortices in the wing/canard configuration, observed in Fig. 4 and in Ref. 6. The connection between the vertical position and the suction has been demonstrated in various basic models of vortex flow over a delta wing.[8,9] It has been shown that a decrease in the vertical component of the wing vortices is accompanied by a decrease in the suction that

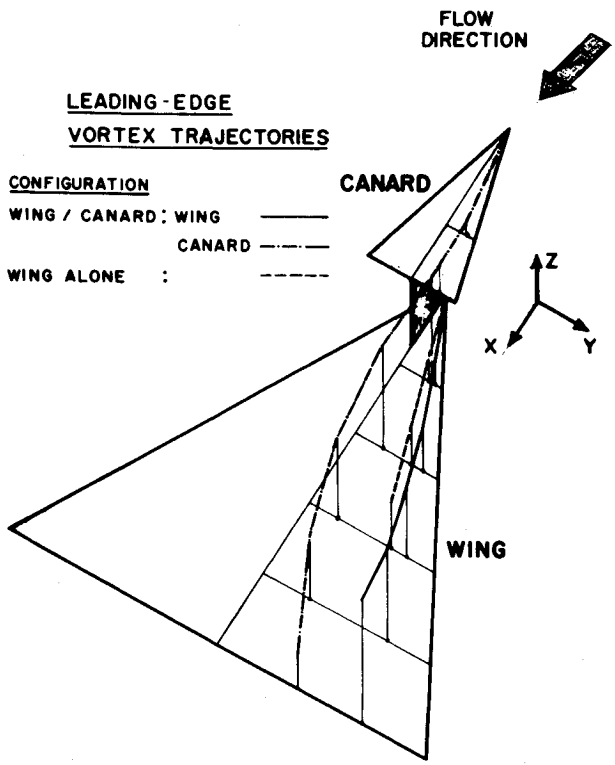

Fig. 4 Qualitative three-dimensional view of the starboard side leading-edge vortex trajectories of the wing and the canard in the wing/canard configuration and of the wing in the wing-alone configuration.

they induce. At higher angles of attack, represented by $\alpha \cong 26$ and 32 deg (Figs. 3c and 3d), $C^u_{p,\min}$ of the wing-alone configuration is smaller near the apex than those of the wing/canard configuration. At these angles, the vortices of the wing-alone configurations are affected by vortex breakdown in the vicinity of the apex, whereas those of the wing/canard configurations are not.[6] This indicates that at these conditions, the balance of the two canard-presence effects (inducing downwash and delaying vortex breakdown), results in larger maximum suction in the wing/canard configuration.

In the center region of the wing (represented by $\bar{x}=0.7$), the canard presence causes an increase in the maximum suction at $\alpha=10$, 18, and 26 deg (Figs. 3a–3c) and a reduction at $\alpha=32$ deg (Fig. 3d). In this region, the vertical position of the wing vortices is higher in the wing/canard configuration. In addition, the wing vortices in the wing/canard configuration are affected by vortex bursting at $\alpha>27$ deg (see Ref. 6) compared to $\alpha>17$ deg in the wing-alone configuration. Thus, increased suction in the wing/canard configuration exists when the wing vortices of this configuration are not affected by vortex breakdown.

In the trailing-edge region (represented by $\bar{x}=0.95$), the canard presence has, in general, a similar effect to that observed in the wing center region. However, the magnitude of the suction induced by the wing vortices is small on both the wing-alone and the wing/canard configurations because of the Kutta condition that prevails at the trailing edge. At $\alpha=26$ deg, an additional suction peak, inward to the one induced by the wing vortices, is observed in the spanwise C^u_p profile of the wing/canard configuration. The vortex trajectory data in Ref. 6 indicates that this additional low-pressure region is induced by the canard vortices that are close to the wing surface for this incidence and chordwise location. Note that, although the canard is considerably smaller than the wing, its vortices at these conditions induce more suction than the wing vortices, due to their proximity to the wing surface. At $\alpha=32$ deg, the wing vortices in both configurations, as well as those of the canard, are affected by vortex breakdown, and the spanwise C^u_p profiles resemble those observed at the same incidence at $\bar{x}=0.7$.

Effects of Canard Sweep Angle

The canard sweep angle influences both the position of the suction peaks and their magnitude. This is demonstrated in Fig. 5, which show the spanwise C^u_p profiles of the wing/canard configuration with the MS canard and the configuration with the HS canard in the forward position. In the apex section of the wing (represented by $\bar{x}=0.25$), the spanwise position of the suction peaks in the wing/MS canard configuration is outboard of that in the wing/HS canard configuration. In this region, the MS canard presents a larger spanwise obstruction to the oncoming flow, generating a larger spanwise flow deflection that displaces the suction peaks outward. At the trailing edge, the spanwise position of the suction peaks of both configurations is almost equal, implying that the additional outboard displacement of the wing vortices in the aft section of the wing is greater for the HS canard than for the MS canard. Evidently, the interaction between the wing and canard vortices in the aft section of the wing is stronger when the canard is highly swept due to its stronger vortices.

The magnitude of $C^u_{p,\min}$ induced by the wing vortices on the wing planform in the wing/MS canard configuration is, in general, only slightly smaller than in the wing/HS canard configuration (Fig. 5). The small difference is consistent with the small difference in the vertical positions of the wing vortices of these two configurations.[6]

The low-pressure regions induced by the canard vortices, which are clearly observed in the surface pressures of the configuration with the HS canard ($\bar{x}=0.7$ at $\alpha=26$ deg), are not evident in the wing/MS canard configuration. This is a consequence of the weaker leading-edge vortices of the MS canard that are also affected by vortex breakdown for $\alpha>10$ deg (see Ref. 6).

Effects of Canard Longitudinal Position

The effects of the canard longitudinal position are studied here on the two configurations with the HS canards, which differ only in the longitudinal position of the canard. Figure 6 shows spanwise C^u_p profiles of these configurations at $\bar{x}=0.25$, 0.7, and 0.95. In general, the characteristics of the pressure profiles are similar in the two configurations, although the magnitude of $C^u_{p,\min}$ in the suction peaks induced by the wing vortices is smaller when the canard is in the rear position. In this configuration, the canard induces downwash on a larger area of the wing apex and appears to inhibit the downstream development of the leading-edge vortices.

The suction peaks induced by the canard vortices are evident on both configurations at $\alpha=26$ and 32 deg (Figs. 6c and 6d). The influence of the canard longitudinal position is observed in the spanwise C^u_p profile at $\alpha=29$ deg and $\bar{x}=0.9$ (Fig. 7). When the canard is in the rear position, the suction induced by its vortices appears to be consistent with vortices affected by vortex breakdown, whereas when the canard is in the forward position, the suction is characteristic of unaffected vortices. This implies that when the canard is in the rear position, its vortices are affected by vortex breakdown at a lower angle of attack. The consequences of this earlier onset of vortex breakdown are discussed in the following section.

Forces and Moments

The spanwise profiles of the pressure coefficients were integrated numerically using the Romberg integration scheme, to produce the wing normal force coefficient and the wing pitching moment coefficient. The values of C^ℓ_p used in the

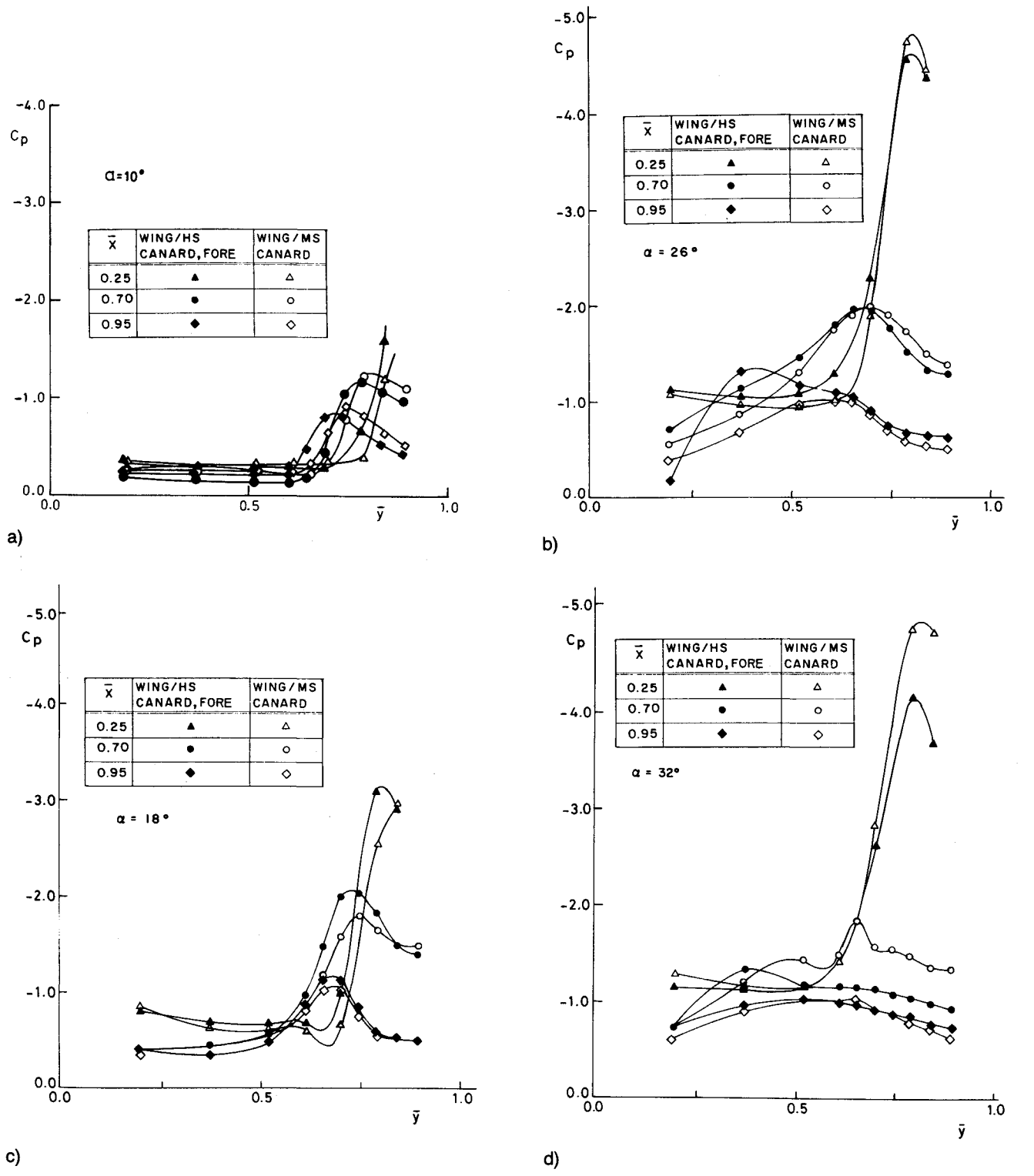

Fig. 5 Spanwise pressure distributions of the wing/MS canard and the wing/HS canard in the forward position configurations: a) $\alpha = 10$ deg. b) $\alpha = 18$ deg. c) $\alpha = 26$ deg. d) $\alpha = 32$ deg:

integration are those measured in Ref. 7 for the wing-alone configuration at the corresponding angles of attack.

Figures 8 and 9 show the wing C_N and C_M curves of the configurations studied in this work. Up to the maximum angle of attack tested in this study, C_N of the wing-alone increases with incidence (Fig. 8) and is in good agreement with the results obtained by Earnshaw and Lawford[10] for a delta wing having a 60 deg sweep angle. The wing C_N of the wing/MS canard configuration also increases with angle of attack and its curve is similar to that of the wing alone, except at the vicinity of $\alpha = 32$ deg, where $dC_N/d\alpha$ of the wing/canard configuration decreases to approximately null. The C_N curve of the wing/HS canard configurations attain a maximum at $\alpha = 25$ deg when the canard is in the rear position and at $\alpha = 29$ deg when it is in the forward position. These maxima appear to be correlated with the breakdown of the canard leading-edge vortices above the upper surface of the main wing. Thus, when the HS canard is employed, the loss of C_N due to the break-

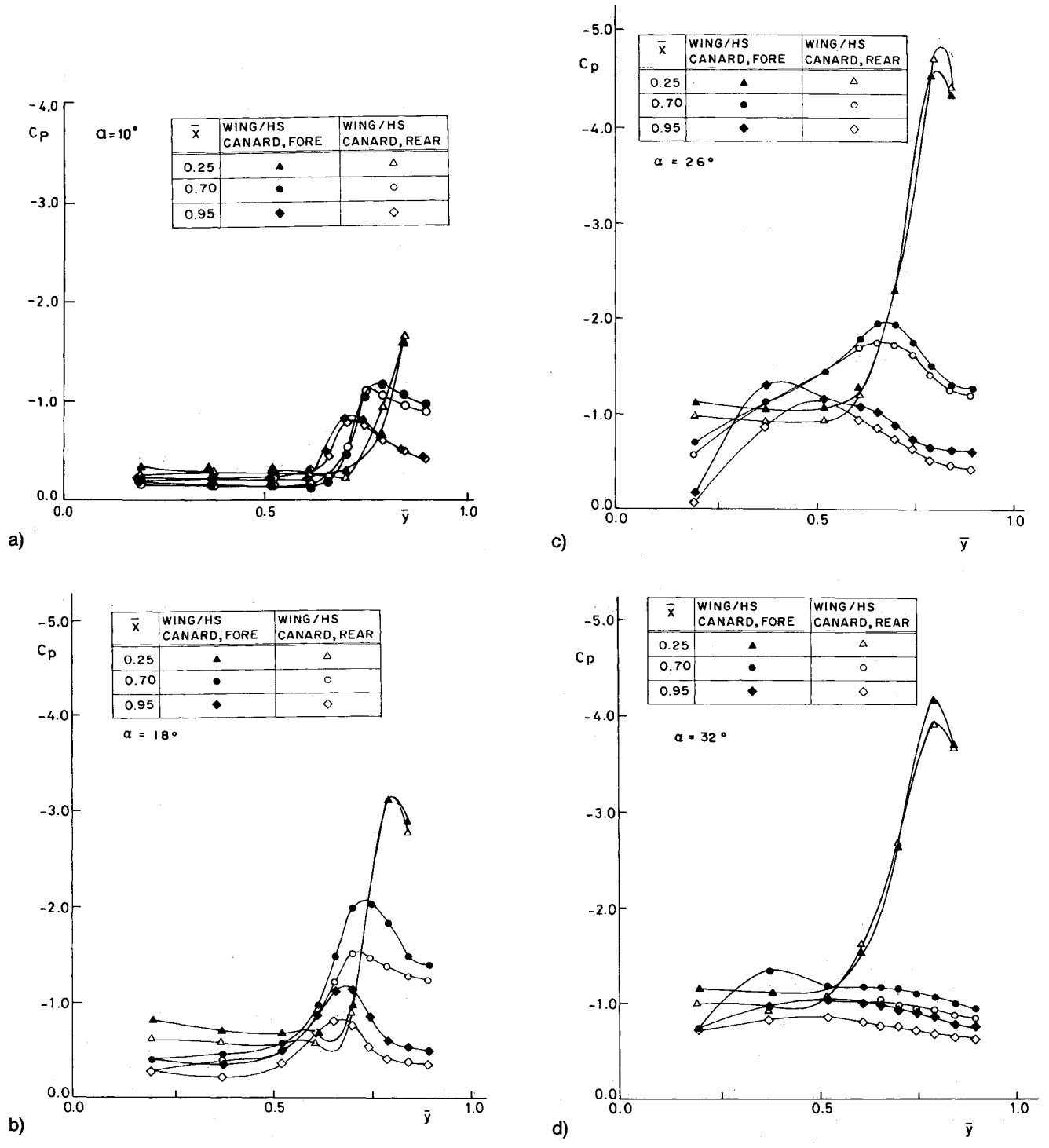

Fig. 6 Spanwise pressure distributions of the wing/HS canard configurations: a) $\alpha = 10$ deg. b) $\alpha = 18$ deg. c) $\alpha = 26$ deg. d) $\alpha = 32$ deg.

down of its vortices causes stall in the wing. Up to the respective stall angles, the wing C_N of the wing/HS canard configuration is, in general, larger than that of the wing-alone when the canard is in the forward position, and smaller when it is in the rear position. Evidently, the reduced suction of the wing vortices when the HS canard is in the rear position results in a decrease in wing C_N in this configuration. In the poststall angles, the wing C_N of the wing/HS canard configuration is smaller than that of the wing-alone.

The wing C_M curves of all configurations are in the negative range (Fig. 9) for the angle-of-attack range studied here. The wing C_M of the wing/MS canard and the wing-alone configurations decreases monotonously with incidence, whereas that wing C_M of the wing/HS canard configurations decreases with incidence up to the stall angles of the respective configurations.

Conclusions

The wing/canard interference mechanism was found to affect the pressure field on the upper surface of the wing, especially the suction induced by the wing leading-edge vortices. This mechanism consists primarily of the following two components: 1) the downwash induced by the canard on the wing apex region and 2) the interaction of the wing and the canard vortices downstream of this region. The contribution of these two components to the wing normal force can be positive or

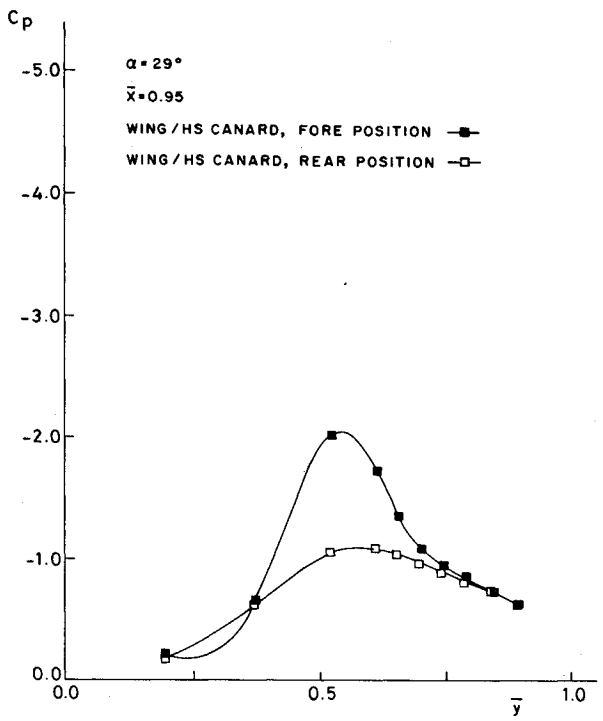

Fig. 7 Spanwise C_p^u profiles at $\bar{x}=0.90$ and $\alpha=29$ deg for the two wing/HS canard configurations.

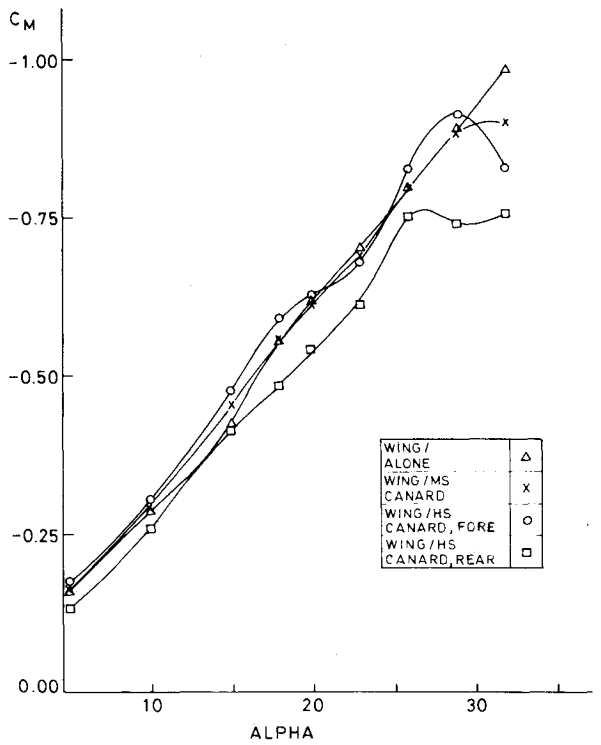

Fig. 9 Wing pitching moment coefficient vs angle of attack.

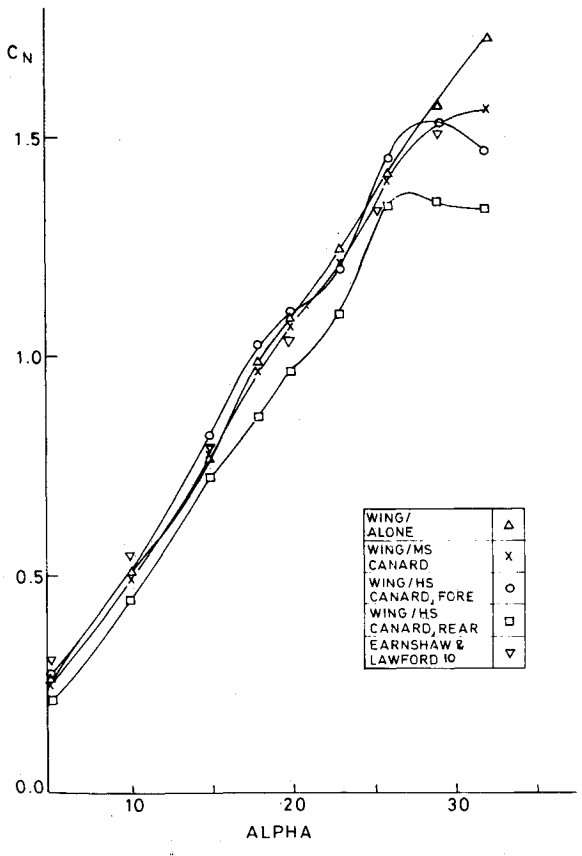

Fig. 8 Wing normal force coefficient vs angle of attack.

negative depending on the angle of attack, canard location, and canard sweep angle.

The direct effect of the canard vortices can be significant when the canard sweep angle is large. For some configurations, the canard induces suction direction on the wing surface and the breakdown of its vortices above the surface of the main planform is followed by the stall of the configuration. These effects are not observed for moderately swept canard configurations in which the canard vortices are weaker.

Acknowledgment

The author would like to thank Mr. Y. Zohar for his assistance in this study.

References

[1]Behrbohm, H., "Basic Low Speed Aerodynamics of the Short Coupled Canard Configuration of Small Aspect Ratio," SAAB Aircraft Co., Linkoping, Sweden, Rept. SAAB TN-60, July 1965.

[2]Gloss, B.B. and McKinney, L.W., "Canard-Wing Lift Interference Related to Maneuvering Aircraft at Subsonic Speeds," NASA TMX-2897, Dec. 1973.

[3]Campbell, J.F., Gloss, B.B., and Lamar, J.E., "Vortex Maneuver Lift for Supercruise Configurations," NASA TMX-72836, Feb. 1976.

[4]Miner, D.D. and Gloss, B.B., "Flow Visualization Study of a Close-Coupled Canard-Wing and Strake-Wing Configuration," NASA TMX-72668, March 1975.

[5]Gloss, B.B. and Washborn, K.E., "A Study of Canard-Wing Interference Using Experimental Pressure Data at Transonic Speeds," NASA TP-1355, Jan. 1979.

[6]Er-El, J. and Seginer, A., "The Leading Edge Vortex Trajectories and Breakdown Characteristics of Close-Coupled Wing-Canard Configurations," *Journal of Aircraft*, Vol. 22, Aug. 1985, pp. 641-648.

[7]Zohar, Y., "The Effect of Vortex Breakdown on the Pressure Distributions of Delta Wings," M.Sc. Thesis, Technion, Israel, 1984.

[8]Brown, C.E. and Michael, W.H., "Effect of Leading-Edge Separation on the Lift of a Delta Wing," *Journal of the Aeronautical Sciences*, Vol. 21, Oct. 1954, pp. 690-694.

[9]Smith, J.H.B., "Improved Calculations of Leading Edge Separation from Slender Delta Wings," Royal Aircraft Establishment, London, TR-66070, March 1966.

[10]Earnshaw, P.B. and Lawford, J.A., "Low-Speed Wind-Tunnel Experiments on a Series of Sharp-Edged Delta Wings," Aircraft Research Committee, London, R&M 3424, 1966.